applied optics

TWINS: improved spatial and angular phase calibration for holography

Alexey Supikov,[1,*] Michael Mefenza Nentedem,[1] Anders Grunnet-Jepsen,[1,2] and Ronald T. Azuma[1]

[1]Intel Labs, Intel Corporation, 2200 Mission College Blvd, Santa Clara, California 95054, USA
[2]Currently with Luminar Technologies, Orlando, Florida 32826, USA
*alexei.soupikov@intel.com

Received 30 June 2023; revised 20 September 2023; accepted 21 September 2023; posted 21 September 2023; published 9 October 2023

We present TWINS (TWo INclining Slits), a method for characterizing phase spatial light modulators (SLMs), inspired by Young interferometry. TWINS is an elegant and versatile approach, using minimal equipment and alignment. It measures phase response locally rather than globally, both horizontally and vertically, with high resolution and at wide angles. It can also measure beam intensity profiles as directly seen by the SLM. TWINS characterizes the anisotropic aberrations in the mainstream models of liquid crystal phase SLMs, which is crucial to improve hologram quality. Compensating for anisotropic aberrations measured by TWINS improved the image quality of planar holograms by 10 dB.

https://doi.org/10.1364/AO.499387

1. INTRODUCTION

Holographic projectors based on phase-only spatial light modulators (SLMs) have rapidly improved in the past 5 years, in both the SLM hardware and the algorithms that compute the holographic images and characterize the system. Holographic projection offers many benefits, such as virtually unlimited brightness, very high dynamic range, and wavefront shaping capabilities that enable lightweight devices with minimal physical optics to change optical characteristics (e.g., focal distance) programmatically. These advantages are crucial to applications such as AR and VR headsets, automobile head-up displays, portable surface-adaptive projectors, and dynamic digital signs. However, generating high quality holographic images requires measuring and compensating for imperfections in real devices, such as the phase response, beam amplitude profile, and system phase aberrations. Characterizing actual devices is a complex task, often requiring extra optical elements, time-consuming alignments, and many manual steps. In this paper, we introduce TWINS (TWo INclining Slits), a technique inspired by Young interferometry. TWINS is an elegant and versatile method offering four major benefits. First, it is a spatially local method that measures phase response at 10–20 pixels resolution and wide field of view (FOV), both horizontally and vertically, measuring anisotropic aberrations. Local measurements do not require camera image to SLM registration. Second, it measures beam profiles directly on the SLM. Third, it is easy to implement, requiring only a camera for usages with a diffusive projection screen. Fourth, using our new method, we show a 10 dB gain in image quality over existing state-of-the-art characterization approaches.

2. RELATED WORK

There are multiple works on phase SLM calibration [1–12]. All have their pros and cons with respect to a given application. Methods using interferometers, such as Twyman–Green, Michelson, or Mach–Zehnder [2–5,11], achieve high accuracy and solve multiple problems. For example, [11] recovers static aberrations, and [3] acquires spatially varying phase response. The need for extra optical elements, often of high quality, precise alignment, and specific placement of the SLM in the light path, makes them less attractive for quick iterations of experimenting with visual holographic systems. Also, they characterize the SLM in isolation from its target system or application. Methods using the SLM to produce an interference pattern observed by a photodiode or camera, such as self-reference, are easier to use, require minimal additional equipment, and produce good results for visual applications. Some detect intensity changes due to varying diffraction efficiency caused by phase differences [9]. Other approaches include a grating-piston method [7], a subsequent work [8] addressing vibrations, a multi-beam method [12], and a temperature-dependent characterization [10]. Easy-to-use methods [7,8,12] operate in the small target cross-section area of the collimated beam directly reflected by the SLM surface and cannot cover the full FOV defined by the maximum diffraction angle of the SLM. Local methods often rely on precise camera image to SLM pixels registration.

Recent advances in algorithms that compute holograms produce nearly perfect results on simulated idealized systems and attempt to optimize holograms for real holographic display systems. Wirtinger holography [13] triggered rapid development of phase retrieval algorithms based on deep learning tools with

auto-differentiation, made widely available by packages such as PyTorch [14]. Neural holography [15] and hardware-in-the-loop [16] methods extend this approach to characterize an entire real holographic display system with aberrations via a neural network trained on holographic images captured by a camera that are registered and compared against target images. While showing impressive results, they are limited to convolutional regime holograms (such as angular spectrum propagation), are not easily extendable to the far field, and do not tell the user how to calibrate individual components such as the phase response of the SLM. In practice, the image quality of planar visual holograms in the far field depends heavily on accurately characterizing the phase response and the beam profile. Both are usually far from ideal, resulting in image degradation and speckle noise.

3. TWINS METHOD

A. Young's Interferometer Experiment

In the 19th century, Thomas Young's famous double-slit experiment showed that coherent monochromatic light passing through two narrow slits creates a characteristic fringe pattern, due to far field diffraction. This intensity pattern has distances between fringes proportional to the wavelength and inversely proportional to the distance between the slits.

Generally, intensity of the far field diffraction pattern produced by two parallel narrow slits of width a separated by distance d with constant phase shifts φ_1 and φ_2 at each slit (like the tilted beam case [17]) is subject to a cosine distribution, shifted proportionally to the phase difference, with sinc-squared fall-off (refer to Supplement 1):

$$I(x_1) \sim a\,\mathrm{sinc}^2\left(\frac{\pi a x_1}{\lambda z}\right)\left[1+\cos\left(\varphi_1-\varphi_2-\frac{2\pi d x_1}{\lambda z}\right)\right]. \tag{1}$$

This intensity pattern, with a distinctive carrier frequency, enables Fourier analysis to extract the phase difference by following the recipe from [7]. Numerical simulation shows that Eq. (1) holds for both Fraunhofer (image at optical infinity) and free space Fresnel far field approximations (finite distance, 2D FFT of the SLM optical field with added distance-based quadratic phase). Thus, two practical implementations of the method are possible: when an image is projected by a lens onto a CCD sensor placed at the focal plane, or when an image is projected on a diffuse screen directly by the SLM. The latter setup supports off-axis and on-axis illumination and a broad range of distances between SLM and the screen, covering our application domains (we tested several distances between 0.5 and 1.1 m).

B. TWINS: Extending Young's Interferometer for Phase SLM Characterization

Using physical masks with narrow slits causes problems with lighting and alignment, so we instead create *programmable phase slits:* setting slit-like groups of pixels on the SLM to different constant phase levels, where these differ from the background. However, we discovered important differences between physical masks and programmable phase slits.

First, the fringes created by programmable phase slits on an SLM experience *half the lateral shift of that created by the physical mask*. To show that, we take the Fourier transform of the source plane optical field, where a SLM of size W has background phase shift φ_0 and two parallel narrow rectangles (phase slits) with *additional* phase shifts of φ_1 and φ_2:

$$\mathcal{F}\left\{\begin{array}{c}\mathrm{rect}\left(\frac{x_0}{a}-\frac{d}{2}\right)\left(\exp(i[\varphi_1+\varphi_0])-\exp(i\varphi_0)\right)\\ +\,\mathrm{rect}\left(\frac{x_0}{a}+\frac{d}{2}\right)\left(\exp(i\,[\varphi_2+\varphi_0])-\exp(i\varphi_0)\right)+\mathrm{rect}\left(\frac{x_0}{W}\right)\exp(i\varphi_0)\end{array}\right\}\left(\frac{x_1}{\lambda z}\right)$$
$$=\exp(i\varphi_0)\left\{a\,\mathrm{sinc}\left(\frac{\pi a x_1}{\lambda z}\right)\left[\left(\exp(i\varphi_1)-1\right)\exp\left(-\frac{i\pi d x_1}{\lambda z}\right)+\left(\exp(i\varphi_2)-1\right)\exp\left(\frac{i\pi d x_1}{\lambda z}\right)\right]+W\mathrm{sinc}\left(\frac{\pi W x_1}{\lambda z}\right)\right\}. \tag{2}$$

The last term in the curly brackets is the zeroth order spot, and the fringe pattern is defined by the expression inside the square brackets, which using [18] can be re-written:

$$2\sin\frac{\varphi_1}{2}\exp\left\{i\left(\frac{\varphi_1+\pi}{2}-\frac{\pi d x_1}{\lambda z}\right)\right\}+2\sin\frac{\varphi_2}{2}\exp\left\{i\left(\frac{\varphi_2+\pi}{2}+\frac{\pi d x_1}{\lambda z}\right)\right\}$$
$$=2\exp(i\Psi)\sqrt{\sin^2\frac{\varphi_1}{2}+\sin^2\frac{\varphi_2}{2}+2\sin\frac{\varphi_1}{2}\sin\frac{\varphi_2}{2}\cos\left(\frac{\varphi_1-\varphi_2}{2}-\frac{2\pi d x_1}{\lambda z}\right)}. \tag{3}$$

According to Eq. (3), the intensity of the fringe pattern of programmable phase slits has cosine distribution with fringes shifted exactly by half of the phase difference between slits. The contrast depends highly on the difference between the phase values in the slits and in the background. Therefore, adjusting background phase can maximize contrast.

Second, since the entire SLM surface modulates light, the far field image is contaminated by a zeroth-order spot and effects of static phase aberrations. These appear as a relatively bright cross shape in the center of the image. Although optical infinity and finite distance setups are affected differently, these problems render images located close to the central axes useless (see Fig. 1 for a real image). To solve this problem, we *shift the far field fringe pattern away from the central axes by introducing a binary diffraction grating pattern inside the slits* (Fig. 2). To ensure consistent

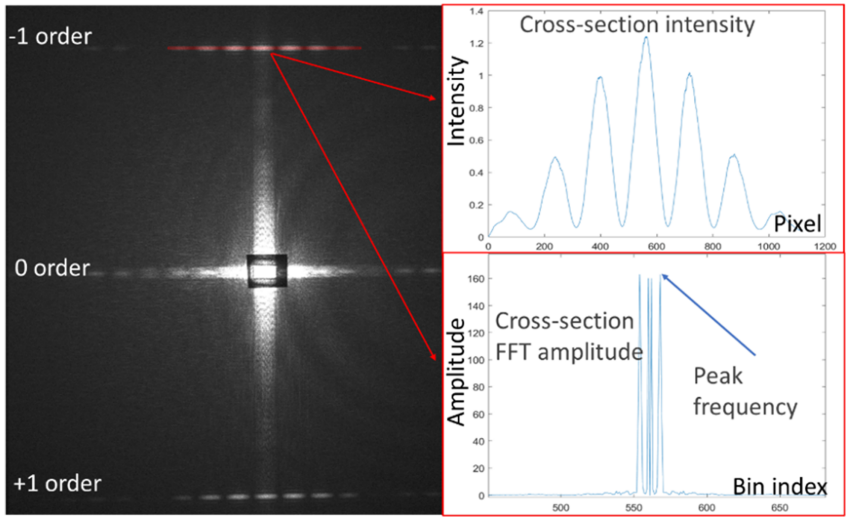

Fig. 1. TWINS fringe pattern image, averaged and filtered cross-section, and its FFT.

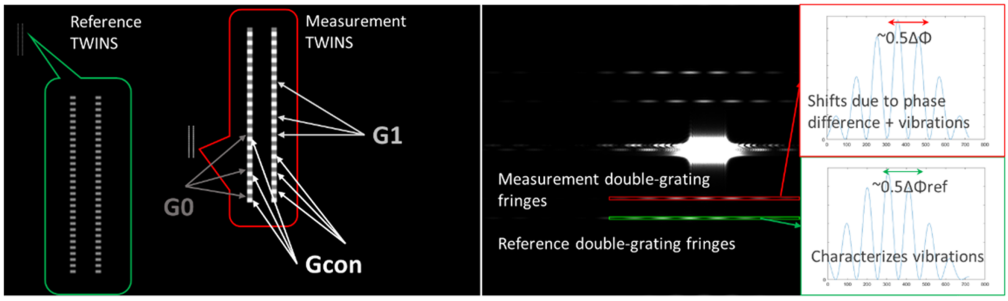

Fig. 2. Left: hologram with measurement slits (red outline) and reference slits (green outline). Right: simulated far field image of the hologram with intensity charts.

patterns and phase shifts, the periods of the gratings are the same for both slits, where the "off" pixels of the grating are set to a common phase value, while "on" pixels are set to the measured phase difference.

Because such narrow grating patterns act like double slits diffracting light away from the central axis, we refer to our method as *TWo INclining Slits*, or *TWINS*.

To measure differences in the phase produced by gray levels $G0$ and $G1$, we set "on" pixels to $G0$ in one slit and to $G1$ in another, with "off" pixels in both slits to a common level G_{con}. The phase produced by level G_{con} should have sufficient contrast with phases from $G0$ and $G1$ to make the fringe pattern in the $+1$, -1 orders bright. For example, for an SLM with 256 phase levels, G_{con} can be around $G0 + 128$. Please refer to the slits in the red outline in Fig. 2.

To measure a phase response curve at one location on the SLM, we set $G0 = 0$ and iterate over the entire grayscale range with $G1 \in [1, G_{\max}]$. One more modification is needed to avoid the fringe pattern disappearing when $G1$ is close to G_{con} (so the grating stops working). We change $G0$ every N_{hop} increments of $G1$ to $G0 = G0 + N_{\text{hop}}$ and update G_{con} to the new $G0 + 128$. We call this modification *base hopping* because it changes the *base level* $G0$. Every N_{hop} measurement reconstructs part of the response curve. We assemble the adjacent parts to generate the full response curve, starting from the first piece.

Predicting where the fringe pattern appears as viewed by the detector camera in a real system is difficult, so the user views and manually specifies the approximate location of the first observed pattern. Due to the approximate selection, measurements contain an additional constant phase shift that we eliminate for each new hop by measuring the phase for both slits set to $G0$, G_{con} and subtracting that from all subsequent measurements in the hop.

TWINS is a spatially local method that detects anisotropic phase response. We can move the slits across the SLM in a finely spaced grid pattern to measure phase response in detail across most of the SLM. We can also orient the slits vertically or horizontally. This detects anisotropic phase response characteristics common in liquid crystal (LC) SLMs.

C. Vibration Compensation and Noise Filtering

TWINS is resilient to many noise sources but is susceptible to vibrations, due to accumulating error when assembling the response curve in base hopping. Vibrations are most noticeable at finite distances when the screen is relatively far from the camera or at optical infinity, when the sensor and projection lens are not rigidly connected to the SLM. We solve this problem by using an auxiliary pair of *reference slits* (marked by a green outline in Fig. 2) located away from the measurement slits to

minimize interference between them. We typically place reference slits approximately half of the SLM width/height away from the *measurement slits* (marked by a red outline in Fig. 2). If the width, length, and spacing of both slit pairs are the same, then the far field image produced by two pairs of slits placed on a constant background will contain two distinctive sets of similar fringe patterns with the same carrier frequency (see Fig. 2, right). Both reference slits "on" and "off" levels are set to some constant values G_{ref}, $G_{\text{ref}} + C$ (C is added to have a contrast phase with G_{ref}). At each measurement step, the phase extracted by Fourier analysis from the reference slit encodes a constant shift plus shifts due to vibration. We can directly subtract the vibration component of the reference phase from the measurement.

If the SLM is physically too small to make the measurement and reference patterns clearly distinguishable, then we provide a different period to the reference slit gratings so the reference fringe pattern will have different diffraction angles from the measurement's. Figures 3 and 4 show the efficiency of vibration compensation in both simulation and a real environment.

In practice, the slits are very small, so the fringe patterns contain significant noise, including speckle. We mitigate the problem with two additional steps. First, instead of using one central cross-section line of the fringe pattern, we average multiple lines (up to 10) around it. Based on extensive simulation, the precision of phase response recovery due to averaging is practically unaffected (error $< 1\%$). Second, we filter the 1D intensity curve generated by averaging before performing Fourier analysis to eliminate effects of speckle noise.

4. ANALYSIS

A. Phase Response Measurement

We use an electrically controlled birefringence (ECB) device with parallel alignment direct voltage driven liquid crystal on silicon (LCoS) phase SLM in a setup detailed in Section 5. The display projects onto a white diffuse screen 1.1 m away from the SLM. We compared phase response curves measured by TWINS with [8] (the vibration compensated variant of [7]). Figure 5 shows the results. When TWINS slits are oriented orthogonal to the rubbing direction [Fig. 5(b)], the curves are very similar to those collected with the global method [8]. There is a slight difference between the curves for the $+1$ and -1 orders, but the mean curve is very similar, providing comparable improvements in the far field holographic images. The difference comes from three key differences of TWINS and [8]. First, TWINS is a spatially local method measuring phase differences between small groups of pixels, while [8] is a global method measuring cumulative differences for a quarter of the SLM. Second, the fringe period expressed in CCD pixels is larger for TWINS, so the resolution is different. Third, TWINS can measure phase modulation performance at wider FOVs than [7,8], which we will show is crucially important for LC-based SLMs.

B. Angular Phase Anisotropy of an ECB LCoS Phase SLM

A typical parallel alignment ECB LCoS SLM in rest state has LC molecules arranged almost parallel to the rubbing direction.

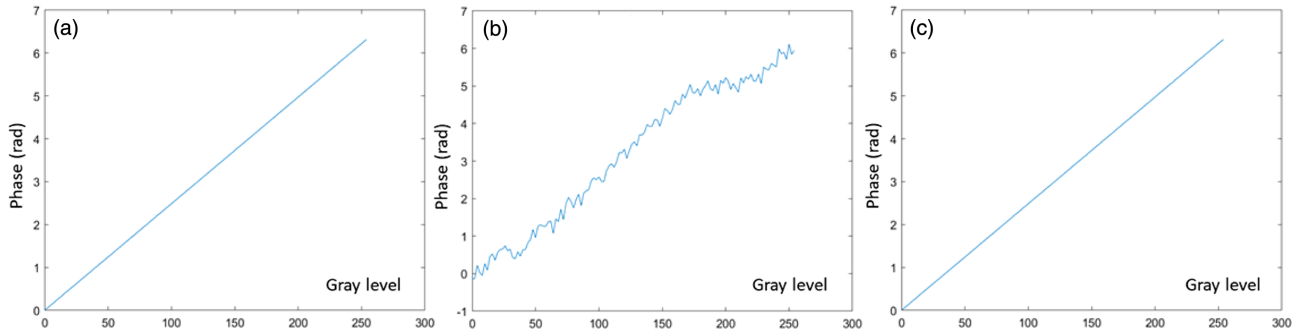

Fig. 3. Simulated phase response measurement by TWINS with emulated vibrations. (a) TWINS simulation, ground truth phase response. (b) TWINS simulation with no vibration compensation, recovered phase response. (c) TWINS simulation with vibration compensation, recovered phase response.

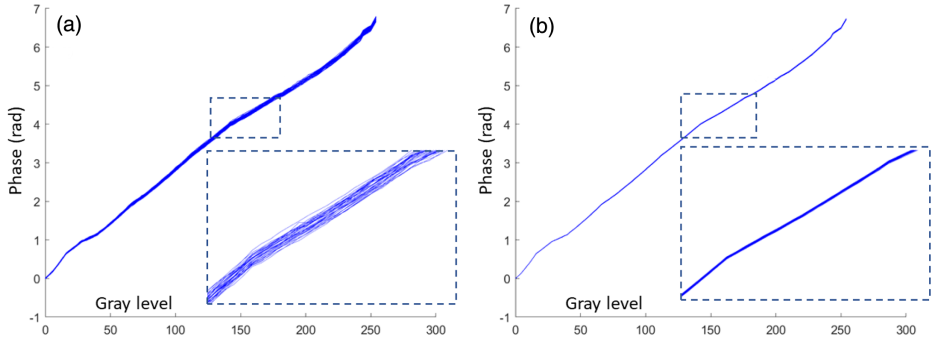

Fig. 4. 30 phase response measurements by TWINS on real setup. (a) 30 real setup experiments with no vibration compensation, recovered phase response. (b) 30 real setup experiments with vibration compensation, recovered phase response.

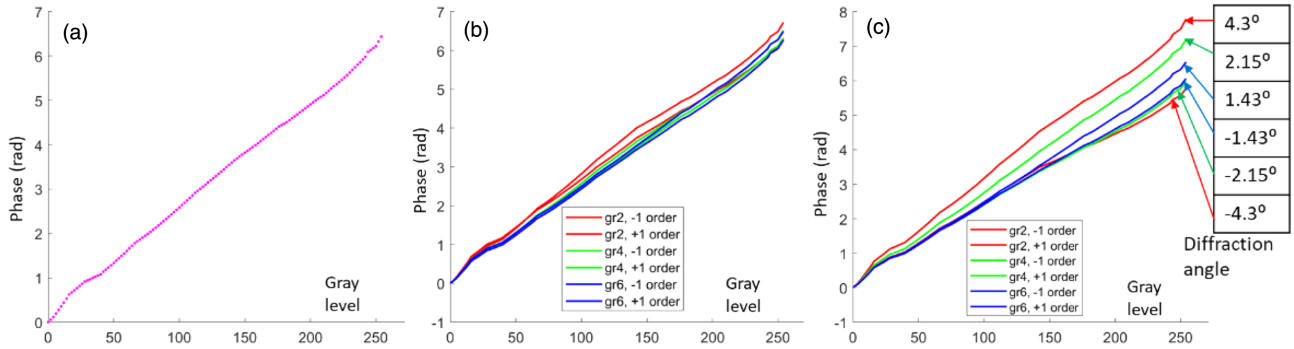

Fig. 5. Phase response measurement: (a) baseline using [7,8], (b) using horizontal TWINS, and (c) vertical TWINS (diffracted along rubbing direction).

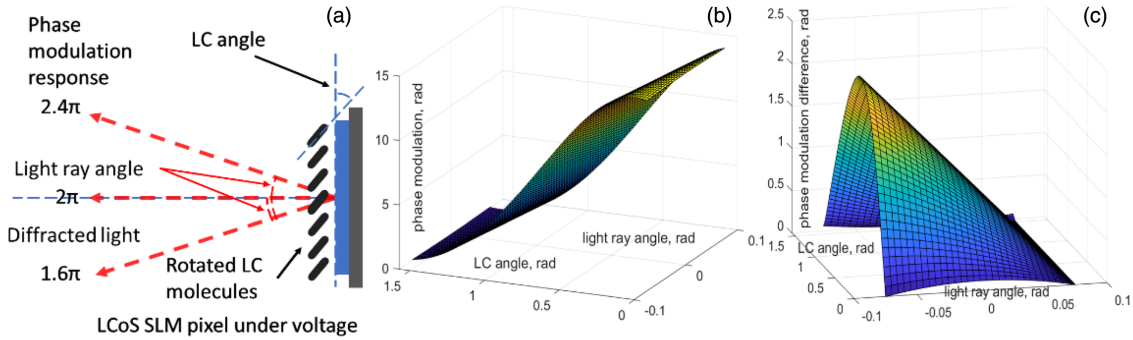

Fig. 6. Modeling anisotropic phase response: (a) simplified LCoS pixel model, (b) phase modulation response, and (c) phase response variation at each LC angle (each voltage level).

Applying voltage rotates the molecules out of the SLM plane, but they remain parallel to each other [Fig. 6(a)]. Light passing through an LC layer in different directions experiences different phase delays, depending on the angle between the propagation direction and the LC molecules. This property is known for limiting viewing angles in LC monitors, but it also reduces the image quality of holograms. Simulating LC cells in an analytical model [19] gives an estimate of the angular anisotropy of phase modulation. We modeled a hypothetical 4 um thick LC cell with extraordinary and ordinary indices equal to 1.9135 and 1.535, respectively, assuming light pierces it at a constant angle. Figure 6(b) shows the phase modulation for different orientations of LC molecules at different incidence angles of light. To visualize anisotropy in phase modulation in Fig. 6(c), we subtract the minimum phase delay value for every LC molecule rotation angle (every fixed voltage level). The range of incidence angles exactly corresponds to a maximum diffraction angle of an SLM with pixel pitch of 4.25 μm. The phase modulation for a fixed voltage can vary substantially with light direction.

Angular phase modulation anisotropy affects far field holograms, even with perfectly collimated light arriving perpendicular to the SLM surface, because *light enters and leaves the SLM in different directions*, due to diffraction from the holographic features and propagation through the LC layers.

TWINS detects and measures anisotropic phase modulation along the SLM X and Y directions by using vertical or horizontal slits. In each orientation, TWINS measures phase modulation along six different angles, by using slit gratings of periods 2, 4, and 6 pixels and detecting the +1 and −1 orders for each period. Since molecules rotate in planes orthogonal to the SLM surface along the rubbing direction, the difference in phase modulation is largest when light is diffracted along the rubbing direction. Figures 5(b) and 5(c) show the six response curves collected using TWINS with slits oriented horizontally along the X axis and vertically along the SLM Y axis (rubbing direction). As expected, light diffracted along the rubbing direction [Fig. 5(c)] shows substantial differences in modulation, while light diffracted along the X axis [Fig. 5(b)] shows small differences. The horizontal off-axis light source, combined with a small in-plane rotation of the SLM in its mount, explains the horizontal anisotropic response.

We now evaluate the benefits of TWINS in holography by comparing the holograms optimized with a conventional phase modulation model (isotropic) against holograms optimized with a directional phase modulation model (anisotropic). Images from both hologram types were produced using anisotropic modulation measured by TWINS. Our hardware allows editing voltage lookup tables (LUTs), and we used TWINS to fine-tune the factory LUT to achieve full 2π range in the SLM normal direction. We used a novel hologram computation method producing "anisotropic holograms" to evaluate compensating for anisotropic aberrations measured by TWINS. We modified the Fresnel approximation of the far field integral to use different modulation curves in the vertical direction, since only the vertical direction (the rubbing direction) is noticeably affected by directional anisotropy. To model phase variation in all vertical directions, we linearly interpolate the six measured response curves along the vertical direction to get response

Table 1. PSNR of Images Produced by Combinations of Computed Hologram and Directional Phase Calibration

	Fine-Tuned LUT		Factory LUT	
Hologram type:	**Isotropic**	**Anisotropic**	**Isotropic**	**Anisotropic**
HUD 20	22.7	33.2	16.6	25.2
HUD 28	26.6	39.3	18.4	27.9
Nature 1	22.0	32.2	14.0	23.3

curves for all target angles. See Section 5 for implementation details.

Table 1 summarizes the results. We computed three holograms, called HUD 20, HUD 28, and Nature 1. They were displayed with TWINS phase calibration (fine-tuned LUT) or the original SLM calibration (factory LUT), and with the hologram computed for isotropic aberrations (the regular Wirtinger approach) or our anisotropic hologram. In all cases, these were displayed on an LCoS system with anisotropic phase response.

First, anisotropic aberrations have a major effect on holographic image quality. Holograms computed by standard Wirtinger holography and displayed on an ideal, simulated holographic display with no anisotropic aberrations result in nearly perfect images, with PSNRs above 40 or 50. But in Table 1, standard Wirtinger holograms (the two isotropic columns) result in PSNRs in the teens or 20's. *State-of-the-art hologram computations are severely degraded when displayed on a real LC holographic display with anisotropic aberrations.*

Second, *compensating for anisotropic aberrations, which TWINS enabled, improves the holographic image quality by over 10 dB.* This is seen by comparing the isotropic and anisotropic columns for the fine-tuned LUT condition. Figure 7, left, shows low brightness and noise artifacts in the upper and lower image areas of a traditional isotropic hologram on anisotropic hardware. Our novel anisotropic holograms reclaim diffraction efficiency and reduce noise (Fig. 7, right). Please refer to Supplement 1 for more examples.

Third, we must *combine the benefits from TWINS in both phase modulation and anisotropic hologram computation to achieve the best results.* The anisotropic hologram displayed with the factory LUT does not reach a PSNR of 30. This shows the LUT is also crucial. The TWINS method shows the factory LUT produces phase outputs with a range below 2π across over 50% of directions, which explains the reduced performance.

C. Measuring Beam Intensity Profile

Accurately measuring and compensating for the beam intensity profile noticeably reduces speckle noise in far field holography. While many external devices can measure beam profiles, their use requires calibration to find the correspondence between SLM pixels and the external device's measurements. As a basis for comparison, we consider a "scanning phase grating" approach that generates a grating, 64 × 64 pixels or larger, that diffracts a beam off the SLM onto a lens focused on a photodiode connected to an oscilloscope. The grating is "scanned" across the SLM in a grid-like pattern to measure the profile at different positions on the SLM.

In contrast, TWINS measures the beam intensity profile directly on the SLM without an external photodiode or oscilloscope. Since the TWINS fringe pattern intensity is proportional to the intensity of the beam illuminating the SLM, we can measure beam intensity by extracting the amplitude of the projected pattern at the carrier frequency. "Scanning TWINS" moves the slits in a grid-like pattern across the SLM, but since the slits are smaller than the pattern in the "scanning phase grating" approach, the resolution is higher. We use slits 64 pixels tall,

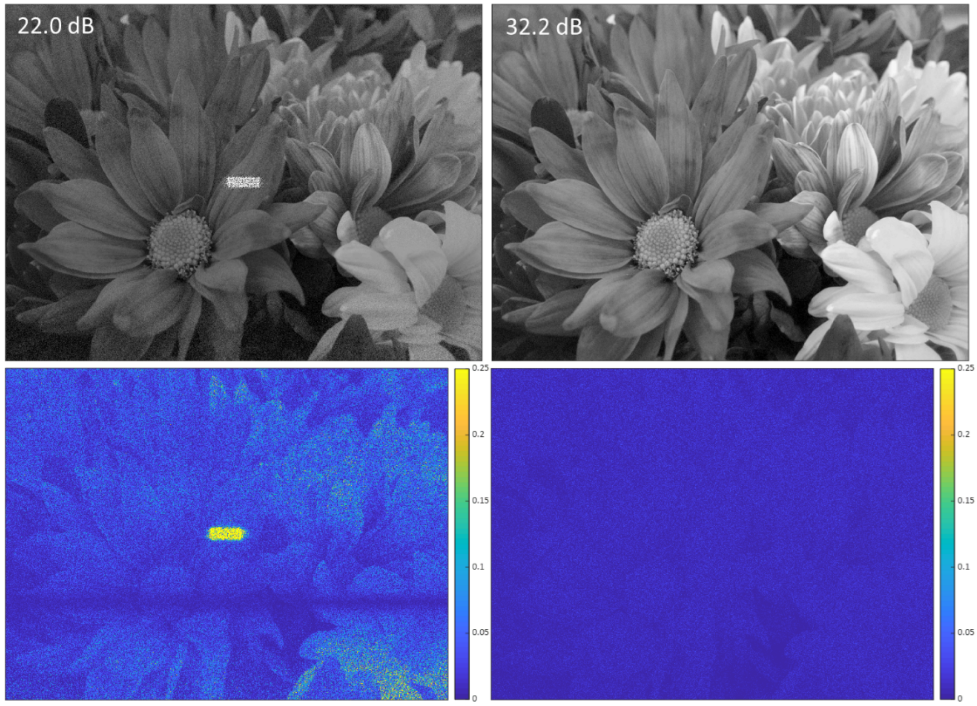

Fig. 7. Isotropic (left) and anisotropic (right) hologram (top) of image Nature 1 on anisotropic LCoS with absolute error maps (bottom).

Fig. 8. Beam profile using scanning grating and photodiode (left) and using vertical TWINS (right).

three pixels wide, and spaced 12 pixels apart. The "scanning TWINS" method requires identifying the area on the diffuse screen to capture, which is done by identifying the projected positions from slits at two opposite corners of the SLM, and the capture window for each position in the grid is interpolated from these extremes.

To get the best resolution of intensity values, we use 12-bit grayscale pixels on the capture camera, adjust the exposure to cover the minimum and maximum intensities, and trigger the camera on the rising edge of the laser beam's "on" signal. The beam intensity profile generated by "scanning TWINS" is very similar to the profile from the "scanning phase grating" method (Fig. 8).

5. IMPLEMENTATION DETAILS

We conducted experiments with a Himax 1920 × 1080 analog LCOS SLM based on HX7322 [20]. The SLM has 4.25 μm pixels and 256 phase levels covering a range of $[0, 2\pi]$. The light source is a red 630 nm LED driven by FISBA ReadyBeam and a Thorlabs 2" achromatic collimator, mounted 4.4° horizontally off axis. Linear polarization of the light is matched with the SLM's rubbing direction. A white diffuse screen was placed at distances between 0.5 and 1.1 m. A Basler a2A5320-23umPRO global shutter camera with 35 mm F/1.8 C-mount low distortion lens captured the projected image on that screen. We attached a small square of black velvet paper to the screen at the location of the zeroth-order spot to prevent sub-surface scattering.

The characterization code runs in MATLAB, generating SLM phase holograms, capturing and processing projected images. A C++ extension displayed holograms on the SLM. We implemented Wirtinger hologram computation in Python, where a PyTorch auto-diff module uses an anisotropic model rather than isotropic, leveraging GPU acceleration in PyTorch.

We modify the Fresnel diffraction integral adding vertically anisotropic phase modulation:

Using the Adam optimizer, we minimize image error searching for proxy phase hologram $P(x_0, y_0)$, subject to vertically anisotropic mapping $P_{\text{map}}[P(x_0, y_0), y_0, y_1]$ transforming SLM phase depending on coordinates y_0, y_1. When computing Eq. (4) with 2D summation using far field FFT-compatible discretization, we use less expensive 1D FFT along the X axis. To ensure the proxy hologram $P(x_0, y_0)$ fits within the SLM grayscale range, P_{map} wraps it around 2π.

6. LIMITATIONS AND FUTURE WORK

TWINS requires a good external camera with a sensor that captures 12-bit grayscale pixels and a low distortion lens. The generated fringe pattern is dim due to the limited number of pixels in the double slits, so this method requires a bright light source. By design, TWINS uses small groups of pixels, which in LC SLMs are vulnerable to fringe fields that smooth the phase. It is difficult to estimate the impact of that smoothing.

The biggest current limitation is that TWINS detects phase relative to the initial phase in the slits and there is no stitching mechanism in place. So, it cannot reliably replace methods measuring static aberrations, such as [10]. In theory and in simulations, a scanning TWINS approach can measure static phase curvature across the SLM. However, a practical implementation requires knowing the exact effect of scanning grating shifts on the fringe pattern. In practice, any error quickly accumulates, introducing unacceptable (> 100%) errors in the measured phase curvature. In addition, the presence of large uncompensated for static phase aberrations introduces crosstalk, affecting measurement accuracy, so slits need to become larger (refer to Supplement 1). We leave it to future work to determine if a practical approach for static phase aberration measurement using TWINS is feasible.

Compensation for anisotropic phase modulation required using summation rather than 2D FFT operations, increasing

$$U(x_1, y_1, z) = C_z \exp\left[\frac{ik}{2z}\left(x_1^2 + y_1^2\right)\right] \iint_{-\infty}^{+\infty} B\,(x_0, y_0)\, \exp(i\, P_m[P(x_0, y_0)\,, y_0, y_1]) \times \exp\left[\frac{ik}{2z}\left(x_0^2 + y_0^2\right)\right] \exp\left[\frac{ik}{z}\left(-x_0 x_1 - y_0 y_1\right)\right] \mathrm{d}x_1 \mathrm{d}y_1. \tag{4}$$

the computation workload due to the quadratic complexity of summation along one axis. Auto-differentiation requires a large memory footprint, so we needed a GPU with 24 GB of memory. Reducing the computation through approximations is a topic for future work.

7. CONCLUSION

TWINS is a novel, elegant, and versatile method for characterizing phase response and beam intensity profiles of an SLM in a holographic display system with minimal additional equipment and automated data collection, making this accessible to all users. It provides similar accuracies to previous work while offering the advantages of measuring locally rather than globally, with high resolution and wide angles, and along several angles both horizontally and vertically. TWINS characterizes anisotropic distortions inherent in LCoS SLMs. Other state-of-the-art approaches could not generate holograms with a PSNR over 30 on hardware with anisotropic distortions. With TWINS, we compensate for anisotropic modulation during hologram computation, improving PSNR by 10 dB to values over 30.

Acknowledgment. The authors thank Qiong Huang for early demonstration of the benefits of the Adam optimizer in holography and Paul Winer for numerous consultations on hardware set up.

Disclosures. AS, AGJ, MMN, RTA: Intel Corporation (P).

Data availability. Due to substantial open-source licensing overhead, the source code underlying the results presented in this paper is not publicly available at this time but may be obtained from the authors upon successful consideration of reasonable request.

Supplemental document. See Supplement 1 for supporting content.

REFERENCES

1. R. Li and L. Cao, "Progress in phase calibration for liquid crystal spatial light modulators," Appl. Sci. **9**, 2012 (2019).
2. Y. Dai, J. Antonello, and M. J. Booth, "Calibration of a phase-only spatial light modulator for both phase and retardance modulation," Opt. Express **27**, 17912–17926 (2019).
3. S. Reichelt, "Spatially resolved phase-response calibration of liquid-crystal-based spatial light modulators," Appl. Opt. **52**, 2610–2618 (2013).
4. M. Lee, D. Koo, and J. Kim, "Simple and fast calibration method for phase-only spatial light modulators," Opt. Lett. **48**, 5–8 (2023).
5. J. Otón, P. Ambs, M. S. Millán, and E. Pérez-Cabré, "Multipoint phase calibration for improved compensation of inherent wavefront distortion in parallel aligned liquid crystal on silicon displays," Appl. Opt. **46**, 5667–5679 (2007).
6. Y. Zhao, W. Yan, Y. Gao, Z. Yuan, Z.-C. Ren, X.-L. Wang, J. Ding, and H.-T. Wang, "High-precision calibration of phase-only spatial light modulators," IEEE Photonics J. **14**, 7402508 (2022).
7. J. L. M. Fuentes, E. J. Fernández, P. M. Prieto, and P. Artal, "Interferometric method for phase calibration in liquid crystal spatial light modulators using a self-generated diffraction-grating," Opt. Express **24**, 14159–14171 (2016).
8. M. Silva-López, N. Uribe-Patarroyo, and A. Álvarez-Herrero, "Advanced iterative algorithm for phase calibration of spatial light modulators integrated in optical instrumentation in a vibration environment," Appl. Opt. **59**, 6760–6764 (2020).
9. O. Mendoza-Yero, G. Mínguez-Vega, L. Martínez-León, M. Carbonell-Leal, M. Fernández-Alonso, C. Donate-Buendía, J. Pérez-Vizcaíno, and J. Lancis, "Diffraction-based phase calibration of spatial light modulators with binary phase Fresnel lenses," J. Disp. Technol. **12**, 1027–1032 (2016).
10. J. Bolek and M. Makowski, "Non-invasive correction of thermally induced wavefront aberrations of spatial light modulator in holographic projection," Opt. Express **27**, 10193–10207 (2019).
11. T. Zhao, J. Liu, X. Duan, Q. Gao, J. Duan, X. Li, Y. Wang, W. Wu, and R. Zhang, "Multi-region phase calibration of liquid crystal SLM for holographic display," Appl. Opt. **56**, 6168–6174 (2017).
12. Y. Gao, R. Li, and L. Cao, "Self-referenced multiple-beam interferometric method for robust phase calibration of spatial light modulator," Opt. Express **27**, 34463–34471 (2019).
13. P. Chakravarthula, Y. Peng, J. Kollin, H. Fuchs, and F. Heide, "Wirtinger holography for near-eye displays," ACM Trans. Graph. **38**, 213 (2019).
14. Pytorch, https://pytorch.org/.
15. Y. Peng, S. Choi, N. Padmanaban, and G. Wetzstein, "Neural holography with camera-in-the-loop training," ACM Trans. Graph. **39**, 185 (2020).
16. P. Chakravarthula, E. Tseng, T. Srivastava, H. Fuchs, and F. Heide, "Learned hardware-in-the-loop phase retrieval for holographic near-eye displays," ACM Trans. Graph. **39**, 186 (2020).
17. R. Fitzpatrick, "Oscillations and waves," 2013, https://farside.ph.utexas.edu/teaching/315/Waveshtml/node75.html.
18. "Sum of complex numbers in exponential form," https://proofwiki.org/wiki/Sum_of_Complex_Numbers_in_Exponential_Form.
19. E. Hällstig, M. Lindgren, and L. Sjökvist, "Study of a nematic zero-twist liquid crystal spatial light modulator," Scientific Report FOI-R-0345-SE (FOI Swedish Defence Research Agency, 2001), https://www.foi.se/rest-api/report/FOI-R–0345–SE.
20. K. H. Fan-Chiang, S. H. Huang, C. Y. Shen, H. L. Wang, Y. W. Li, H. C. Tsai, and Y. P. Huang, "Analog LCOS SLM devices for AR display applications," J. Soc. Inf. Disp. **28**, 581–590 (2020).